THERMAL BEHAVIOUR OF LAMINATED BAMBOO STRUCTURES UNDER FIRE CONDITIONS

Ian Pope*[1], Juan P. Hidalgo[1], Andres Osorio[1], Cristián Maluk[1] & José L. Torero[2]
[1] The University of Queensland, School of Civil Engineering, Australia
[2] University College London, Department of Civil, Environmental and Geomatic Engineering, UK

*Corresponding author: i.pope@uq.edu.au

ABSTRACT

A series of experiments have been conducted to measure the in-depth heating of laminated bamboo samples subjected to heat fluxes of 5, 10, 30 and 60 kW/m^2, either perpendicular or parallel to the grain. These heat fluxes were chosen to induce different phenomena within the material – from inert heating to moisture evaporation, pyrolysis, oxidation and flaming – so that the effects of these can be isolated and evaluated separately by simple heat-transfer models. Moisture migration along the fibres becomes a critical factor when bamboo is heated parallel to the grain, resulting in increased convective heat transfer to deeper parts of the material, and an accumulation of moisture in depth that accentuates the endothermic plateau in the temperature profiles around 100 °C. Average charring rates for 60 minutes of exposure under 60 kW/m^2 were 0.74 and 0.70 mm/min for perpendicular and parallel heating respectively. The thickness of the heated layer was much larger for parallel heating due to moisture migration, which is less significant perpendicular to the grain. Inert heat diffusion is a good approximation at heat fluxes of 5 and 10 kW/m^2, but exothermic oxidation reactions become critical above 400 °C, and must be included in future models.

KEYWORDS: bamboo; laminated bamboo; heat transfer; modelling; charring; temperature measurement; grain orientation; thermal exposure

1. INTRODUCTION

Laminated bamboo is a novel construction material that shares many of the attractive qualities of engineered timber products, such as cross-laminated timber (CLT) or glued laminated timber (glulam), which are becoming increasingly popular for use as primary structural materials in mid- and high-rise buildings. Laminated bamboo structural elements possess a high strength-to-weight ratio, ease of prefabrication, and high aesthetic value, as well as the ability to sequester carbon during growth.[1] Significantly, it may also be more readily available than timber in regions with large populations and developing economies, including Latin America, East Africa, and Asia.[2]

As a combustible material, the use of laminated bamboo in construction has thus far been constrained to secondary applications or low-rise buildings, due to a lack of research and understanding of its fire performance. The main consideration in the structural performance of lignocellulosic materials during a fire is the change in mechanical properties of these materials, as well as their connecting elements, at elevated temperatures.[3] While there are currently no standard design methods for laminated bamboo structures, existing standards for

timber construction prescribe the use of a "reduced cross-section method" in which the effective cross-section of a member is reduced by the progression of a char layer and an additional "zero strength layer".[4] The char layer is bounded by a charring front that is commonly assumed to be approximated by the 300 °C isotherm,[5] due to the peak in mass loss around this temperature as the material pyrolyses.[6] Timber and bamboo share a similar chemical content – with both composed primarily of cellulose, hemicellulose and lignin in similar proportions[7] – so it is likely that this charring approximation may be reasonable for bamboo as well. However, it has been found that both bamboo and timber begin to lose structural capacity at much lower temperatures, with significant changes in both strength and stiffness observed at temperatures that could develop well ahead of the charring front.[3,5,8] The zero strength layer specified by timber design codes is intended to address the additional loss of capacity within this "heated depth", however it may not adequately account for the effect of elevated temperatures on the mechanical properties in bamboo under all possible heating conditions. The inadequacy of applying this method to laminated bamboo has previously been observed,[9] and may in part be due to the higher conductivity of bamboo compared with softwood timbers.[9-11] Therefore, to facilitate the performance-based design of these structures, it is necessary to explicitly consider the temperature profile behind the char layer when predicting material degradation.

This thermo-mechanical analysis requires sufficiently accurate tools for designers to predict the evolution of temperature profiles under relevant fire scenarios. Although no such tools have been developed for bamboo, numerous attempts have been made for timber.[12-14] These studies have shown that in-depth temperatures in lignocellulosic materials under high thermal loads cannot be predicted by purely diffusive heat transfer models, but are also dependent on endothermic and exothermic phenomena. Moisture evaporation, pyrolysis, and oxidation reactions are all additional source terms that may need to be accounted for in the energy equation, along with a transient variation of boundary conditions related to cracking, shrinking and regression of the surface of the material. While generalised models that have the potential to account for all of these effects exist,[15] they are typically of such complexity that they are impractical for design office use. Furthermore, these models may require a large number of input parameters that are not well established, or can only be derived by inverse modelling. The result of this is that models of increasing complexity also suffer from higher levels of uncertainty[16] that limit their applicability beyond the specific scenarios for which they are optimised. An ideal model should therefore be of the minimal complexity required to accurately predict in-depth temperatures, by describing only the most significant fundamental heating mechanisms.

The intent of this study is to enable this kind of simplified model by identifying the most critical source terms that must be included to accurately predict temperature profiles. This is achieved through a series of experiments and accompanying models, which are designed to decouple various phenomena so that they may be analysed separately. In-depth temperatures have been measured in laminated bamboo samples subjected to various heating conditions that result in different phenomena within the material. Low levels of irradiance impose an almost inert heating regime, while higher applied heat fluxes induce increasingly complex combinations of phenomena such as moisture evaporation, pyrolysis (charring) or char oxidation (smouldering combustion). These experimental results are to be used as a benchmark for models of increasing complexity, of which a few purely diffusive models have been presented herein to assess the significance of different source terms. Finally, some experimental temperatures have been used as an input into a model, in the form of a Dirichlet (surface temperature) boundary condition, so that the effects of phenomena occurring outside

of this boundary can be indirectly accounted for and isolated from the heating mechanisms through the rest of the material.

2. EXPERIMENTAL METHODS

The laminated bamboo samples were composed of rectangular-sectioned strips of *Phyllostachys pubescens* (Moso) bamboo – each measuring approximately 7 × 25 mm – arranged into lamellae and bonded together with a phenol-formaldehyde resin to form larger composite sections. The samples created in this manner measured either 120 × 120 × 100 mm or 120 × 120 × 120 mm, depending on whether they were heated perpendicular or parallel to the grain direction. In either case, the exposed surface measured 120 × 120 mm, however a greater thickness was chosen for those samples heated parallel to the grain, because the higher thermal conductivity in this direction[10,11,17] could lead to faster propagation of the thermal wave towards the back of the material. Heating of the rear surface would invalidate the assumption of semi-infinite heating, which allows the rear boundary condition in the model to be greatly simplified, so it is desirable to facilitate this assumption for as long as possible. The average density and moisture content of the samples were found to be approximately 675 kg/m^3 and 7 %, respectively.

The samples were subjected to radiant heat fluxes imposed by a Mass Loss Calorimeter in the vertical orientation, as shown in Figure 1, with the grain oriented either perpendicular or parallel to the incident heat flux. Constant heat fluxes of 5, 10, 30 and 60 kW/m^2 were chosen as they represent distinct heating regimes that result in different physical and chemical phenomena within the material. At 5 kW/m^2, heating was expected to be almost inert, since this is well below the critical heat flux for piloted ignition for laminated Moso bamboo of 14 kW/m^2.[9,18] As such, only some minor endothermic effects due to evaporation of moisture around the 100 °C isotherm were expected, with only minimal pyrolysis. At 10 kW/m^2, low-temperature pyrolysis and effects related to moisture would be present, however no significant charring, surface regression, cracking, or flaming should occur, since this is still below the critical heat flux for ignition. The 30 kW/m^2 heating condition was imposed without the addition of a pilot igniter (to avoid flaming ignition) but all of the aforementioned phenomena would be present, along with smouldering combustion and oxidation of the char layer. Finally, the 60 kW/m^2 heating regime would include all of the burning phenomena to be expected under fully developed fire conditions. A pilot igniter was introduced for this heat flux to ensure that flaming ignition occurred quickly once the sample was exposed, thus having an additional steady heat flux from the flame.

Figure 1. Samples exposed to 60 kW/m^2 perpendicular (left) and parallel (right) to the grain.

The vertical orientation was chosen based on the approach of Reszka[12] to simplify the boundary conditions, as this avoids the issue of two-dimensional convection associated with the horizontal configuration. Moreover, this configuration allows for the rear of the sample to be exposed to the ambient air, eliminating the potential for it to be heated by contact with the sample holder, and allowing the assumption of semi-infinite heating for a longer period. The dimensions of the sample – being larger than those normally specified for the Cone Calorimeter[19] – were chosen to reduce the influence of edge effects, such as radiative heating or flaming along the sides of the sample, to support the assumption of one-dimensional heating near the centre of the sample.

Thermocouples were inserted into the side of the sample at distances of 3, 8, 15, 25, 40, 60 and 80 mm from the heated surface. These in-depth thermocouples were of type K, with a sheath diameter of 1.5 mm, and were inserted into 2 mm diameter holes spaced at least 10 mm apart. The thermocouples were positioned close to the centre of the sample, with three thermocouples located at the 3 mm depth and two each for the remaining depths, all embedded 60 mm in from the sample side. An additional exposed junction thermocouple was placed on the rear surface of the sample, at a distance of 100 or 120 mm from the heated surface (depending on orientation) and fixed to this surface with aluminium tape. The thermocouple sheaths extending from the side of the sample were shielded from radiation, as shown in Figure 1. Experiments at each heat flux were repeated at least twice, with more repetitions for the higher heating rates that had a larger variation, resulting in at least four measurements for each in-depth measurement point, as shown in Table 1. The thermocouples on the rear face were only intended to identify whether the heat wave had reached the back of the sample, so fewer measurement points were required.

Table 1. Number of Repetitions and Measurements for Each Heat Flux

Orientation	Heat flux (kW/m^2)	Repetitions	Aggregate number of measurements for each location		
			3 mm	8, 15, 25, 40, 60, 80 mm	100/120 mm
Perpendicular	60	4	12	8	4
	30	3	9	6	3
	10	2	6	4	2
	5	2	6	4	2
Parallel	60	2	6	4	2
	30	2	6	4	2
	10	2	6	4	2
	5	2	6	4	2

3. EXPERIMENTAL RESULTS

As expected, no significant charring or regression was observed in the experiments conducted at 5 and 10 kW/m^2, although the surface of the sample under 10 kW/m^2 eventually became blackened, indicating a degree of pyrolysis close to this face. Significant charring, cracking, regression, and smouldering combustion was observed at 30 kW/m^2, but there was no flaming ignition since no pilot igniter was introduced. For the 60 kW/m^2 case, piloted flaming ignition occurred approximately one minute after exposure. For the 30 and 60 kW/m^2 cases, oxidation and regression of the char layer eventually resulted in exposure and fallout of those thermocouples initially at depths of 3 and 8 mm. This generally occurred at temperatures of between 700 to 800 °C for 60 kW/m^2 exposure, and 600 to 700 °C under 30 kW/m^2. This difference may be partly due to the lower temperatures required for oxidative reactions at a lower heating rate,[20] as well as the different boundary conditions in each case. Once the thermocouples started to be exposed, their measurements became unsteady as they were increasingly a function of the external gas temperatures. The data for these locations is presented up until the thermocouple readings became distinctly more unsteady, since these are no longer purely solid-phase temperature measurements and should be disregarded. No delamination was observed in any of the experiments, despite multiple glue lines being subjected to temperatures over 300 °C, with only small localised fragments of char observed to fall off from the exposed surface. However, the intent of this study was not to evaluate delamination, which may result under loading conditions that were not replicated in these experiments.

Experimental results are presented in Figures 2 to 4 as averages, with single standard deviation intervals indicated. Values for intermediate depths between measuring points were estimated by interpolation using a shape-preserving cubic hermite polynomial. When describing these results, “shallower” measuring points are those that are closer to the heated surface, while “deeper” points are closer to the rear of the sample. These results show a clear distinction between the behaviour of the material when heated in different orientations. This was observed to some degree across all heat fluxes, although it is most distinctive in the results for higher heat fluxes, shown in Figures 2 and 4. In both cases, an inflexion or plateau is observed in the temperature profiles around 100 °C due to the endothermic evaporation of moisture. In the perpendicular heating case, this inflexion is small but noticeable for the shallower measuring points that were subjected to a higher heating rate, but becomes less significant with depth. Conversely, for the parallel heating case, this effect becomes even more pronounced with depth since moisture can travel and accumulate along the fibres. As the moisture migrates and recondenses ahead of the evaporation front,[12] energy is transferred

from the moisture to the surrounding material, increasing the temperature of this region. This is essentially an additional source of convective heat transfer and mass transport that is inhibited for the perpendicular heating configuration. Bamboo is a variety of giant grass, in which the fibres exlusively run longitudinally along the internode regions, with a small proportion of fibres running transversally inwards only at the nodal diaphrams.[2] As a result, there are no transverse fibres to promote moisture transport perpendicular to the grain over the internodal regions that constitute the great majority of the material. Furthermore, lamination of the strips taken from the narrow bamboo culm wall creates numerous discontinuities in the form of glue lines that are arrayed against the flow of moisture perpendicular to the grain.

Behind the shallowest thermocouple depths, temperatures initially rise more rapidly for heating parallel to the grain. This is partly due to the higher conductivity and therefore higher diffusivity in this direction allowing the heat wave to progress more quickly, but is greatly enhanced by the additional convective effect of the moisture migration. Subsequently, the rate of temperature rise in each location reduces for parallel heating as temperatures approach 100 °C, since endothermic evaporation becomes more significant. Also notable in the parallel heating case is the lower variability in temperatures close to 100 °C, which may suggest the presence of a water-saturated layer moderating temperatures in this region. This saturated layer acts as a significant local heat sink due to the energy required to evaporate the water. For the higher heat fluxes, the eventual temperatures above 200 °C at each depth are higher for perpendicular heating, which may be due to less energy being lost through diffusion towards the cooler end of the material. However, as shown in Figure 3, under 10 kW/m^2 the temperatures for the 3 and 8 mm thermocouples in the parallel heating case rise above their perpendicular heating equivalents after 20 minutes. This is not observed in any of the other heating regimes, but may be caused by some limited smouldering occuring very close to the surface under 10 kW/m^2, once the surface temperatures rise above 200 °C.[6] This exothermic reaction could be exacerbated in the parallel heating case due to the higher permeability in the direction of the fibres allowing greater oxygen diffusion into the material.

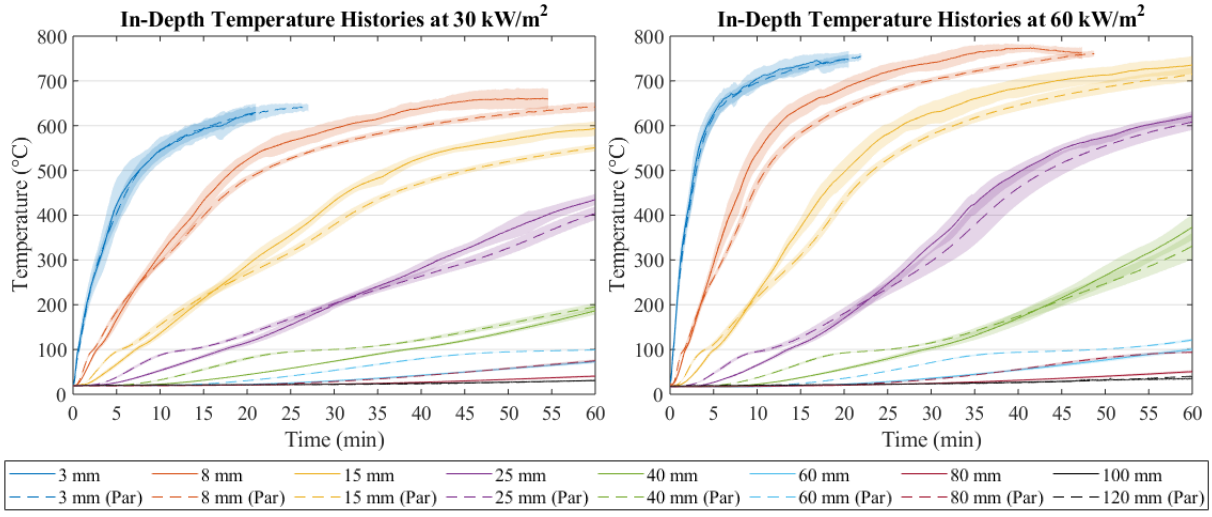

Figure 2. Temperatures at various depths under 30 and 60 kW/m^2 irradiation perpendicular (solid) and parallel (dashed) to the grain. Mean values shown, with standard deviation intervals shaded.

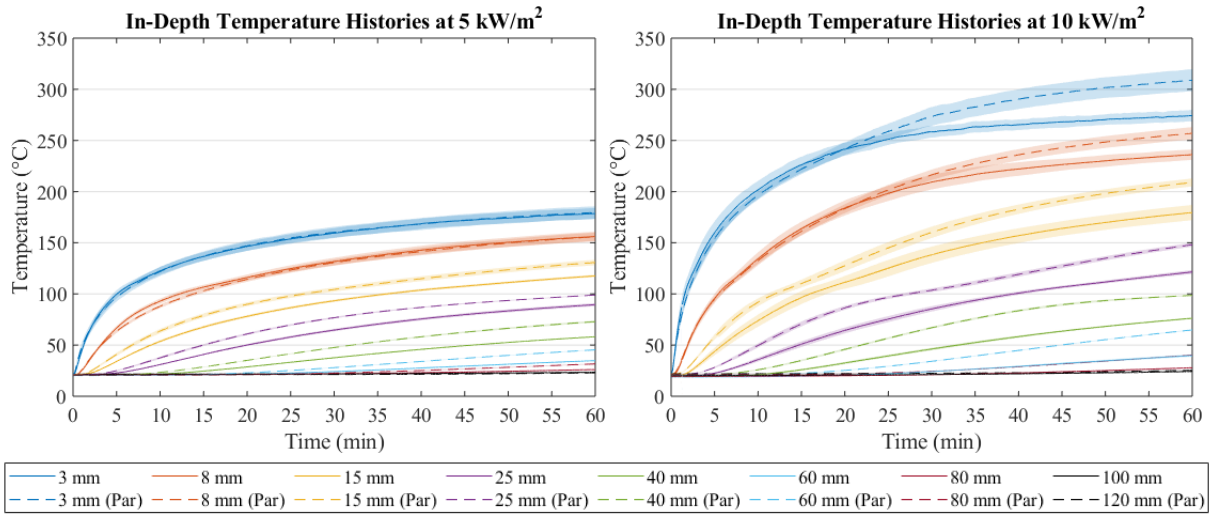

Figure 3. Temperatures at various depths under 5 and 10 kW/m^2 irradiation perpendicular (solid) and parallel (dashed) to the grain. Mean values shown, with standard deviation intervals shaded.

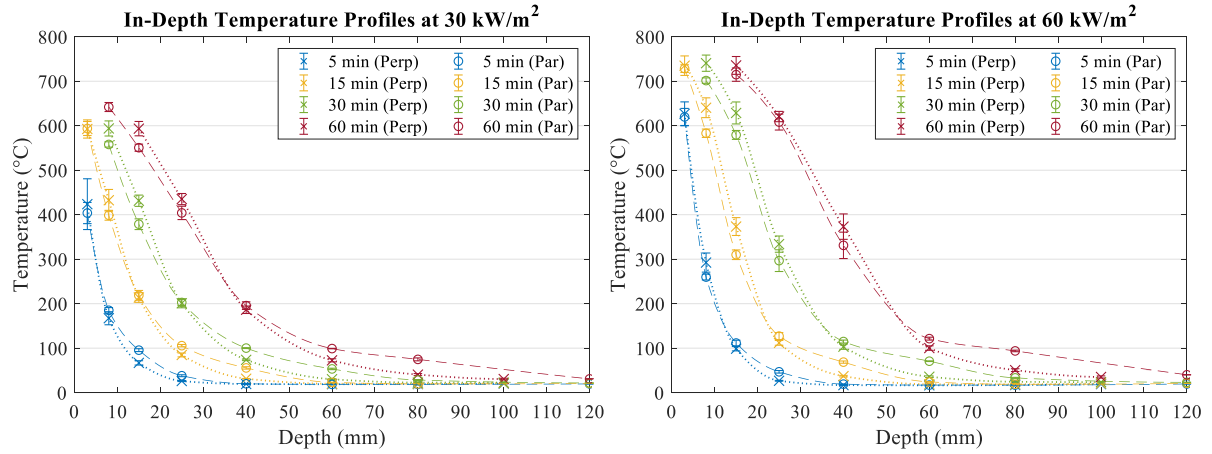

Figure 4. In-depth temperature profiles under 30 and 60 kW/m^2 irradiation perpendicular (crosses) and parallel (circles) to the grain. Mean values shown, with standard deviation intervals indicated.

The effect of the grain orientation can also be seen in the differences in the charring rate and heated depths between these cases. Average charring rates have been calculated for 60 kW/m^2 heating, based on the total distance over which the 300 °C isotherm has moved in different lengths of exposure time. As shown in Figure 5, average charring rates are approximately equal in either case, however the depth at which temperatures begin to rise above ambient is much greater for heating parallel to the grain, potentially leading to earlier material degradation. To illustrate this, the movement of the 60 °C isotherm has been used to track the in-depth heating front, while the thickness of the "heated layer" is calculated as the distance between the charring front and the 60 °C isotherm. The movement of isotherms has been estimated over discrete time intervals by the previously described interpolation between measurement points. This may result in higher errors when the isotherm is far from a measuring point, particularly when the gradient of the temperature profile is small, but the significance of this error is reduced when a trend is evaluated over a series of reported times.

Charring rates peak at the beginning of exposure, before gradually reducing as the char layer

develops. The average charring rate for 60 kW/m^2 heating perpendicular to the grain is approximately 1.55 mm/min after 5 minutes and 0.74 mm/min over 60 minutes, compared with 1.40 mm/min and 0.70 mm/min for the parallel case. However, temperatures below around 200 °C occur at significantly greater depths for the parallel case after the same exposure times. After one hour of heating parallel to the grain at 60 kW/m^2, the heated depth is 105 mm, compared with 74 mm in the perpendicular case. As a result, the thickness of the heated layer after 60 minutes of perpendicular heating at 60 kW/m^2 is around 29 mm, compared with 63 mm in the parallel heating case. This indicates that the onset of mechanical deterioration could occur more than 30 mm deeper into the material for parallel heating under these conditions.

In both cases, the heated layer grows throughout the period of exposure, and does not clearly approach a steady value within the one hour duration. The growth of the heated layer can be closely approximated by a linear regression (with an r-squared value greater than 0.95), from which the rate of growth can be extracted. Between 5 and 60 minutes of exposure, the average rate of growth of the heated layer is approximately 0.34 mm/min perpendicular to the grain, but for parallel heating it is almost three times larger at 0.93 mm/min. This disparity cannot be accounted for by a reduced cross-section method with an assumed zero strength layer, nor by simple heat diffusion models that do not account for the effect of moisture transport and accumulation along fibres running parallel to the heat flow. However, for the perpendicular heating case, it may be possible to neglect this issue since moisture accumulation in-depth is minimised. This would be advantageous since this represents the most common configuration in which laminated bamboo is used in construction. However, the parallel heating case may become critical when the ends of structural members are heated, particularly near connection points between loadbearing members.

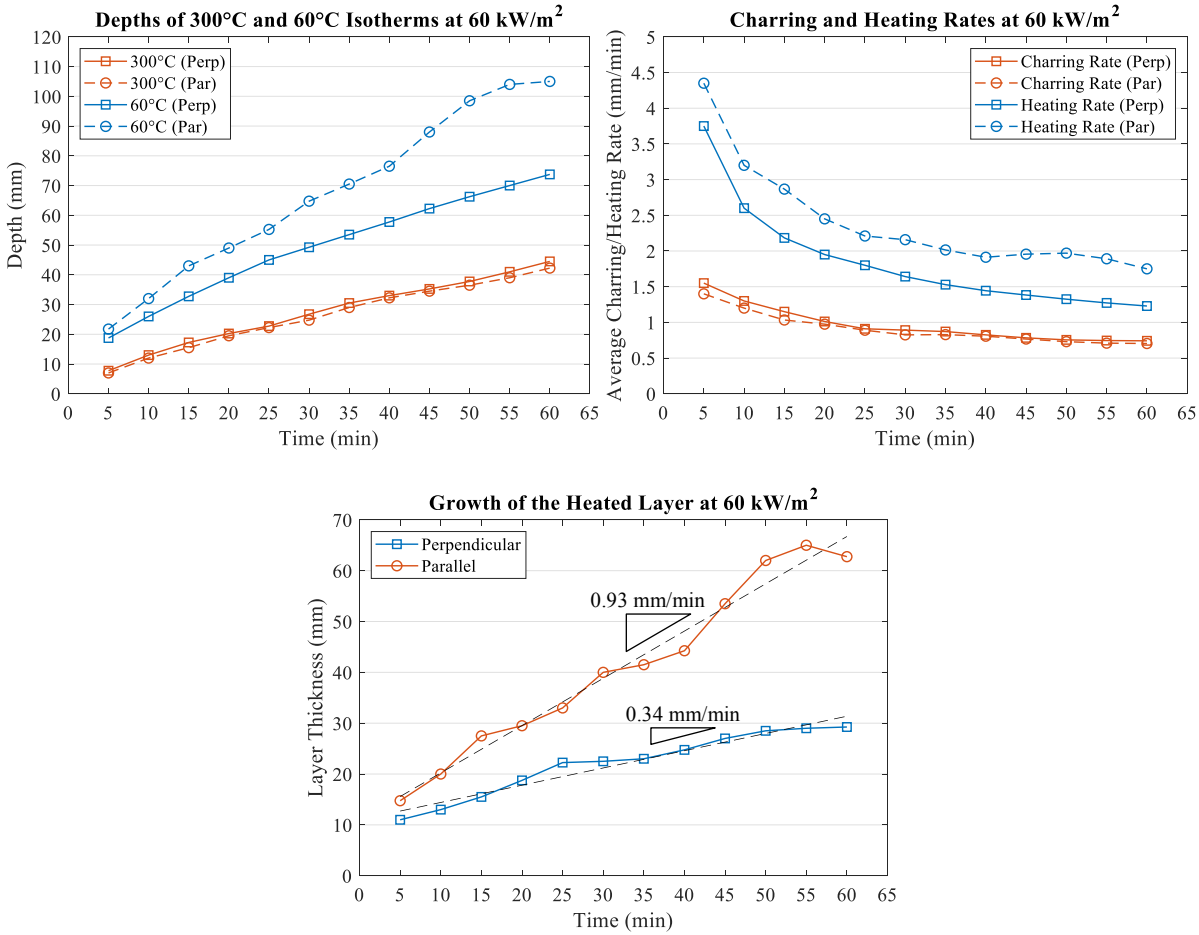

Figure 5. Progression of charring and heated depths, and development of the heated layer under 60 kW/m^2 irradiation perpendicular (squares) and parallel (circles) to the grain.

4. MODELLING APPROACH

The simplest approach to modelling in-depth temperatures is to assume an inert heating regime (i.e. neglecting source terms) with constant material properties. Since bamboo experiences complex reaction mechanisms, changing material properties, and dynamic physical processes under high heat fluxes, this characterisation diverges significantly from reality. Nonetheless, as a baseline, this approach can be useful in identifying how, and under what conditions, the behaviour of the material diverges from purely inert heat diffusion. For this purpose, a one-dimensional finite difference model has been implemented in MATLAB for use as a baseline at each heat flux. Initially, material properties are assumed to remain constant at their ambient temperature values, with all model inputs obtained either by direct measurement, taken from literature,[9,10,14,21] or assumed as shown in Table 2. Some subsequent models utilise moving boundary layers with different material properties in each region, and these are also included. As seen in the experimental results, heating along the grain appears to be highly influenced by moisture transport along the fibres. However, the intent of this study is not to investigate the specific mass and heat transfer phenomena associated with this, so the results of the models – which do not account for these effects – are compared only with the experiments in which heat was applied perpendicular to the grain.

Table 2. Input Parameters and Assumptions for Heat-Transfer Models

Input parameter		Value or condition
T_∞	Ambient temperature	Measured ambient temperature during experiments (23-26 °C)
T_0	Initial temperature	Measured initial sample temperature (18-21 °C)
$\dot{q}''_e$	Incident radiation	5, 10, 30 or 60 kW/m^2
$\alpha = \varepsilon$	Absorptivity/emissivity	0.9
$\dot{q}''_{l,r}$	Emitted radiation	Stefan-Boltzmann Law
$\dot{q}''_{l,c}$	Convective cooling	Relationship for a vertical flat plate in quiescent air[21]
MC	Moisture content	7 %
Rear boundary condition		Adiabatic (no heat losses)

Thermal properties:	Conductivity (W/m·K)	Density (kg/m^3)	Heat capacity (J/kg)
Ambient (below 100 °C)	$k = 0.25$ [10]	$\rho = 675$	$C_P = 2260$ [9]
Dry (100 to 300 °C)	$k_d = 0.95k = 0.24$ [14]	$\rho_d = (1\text{-}MC)\rho = 628$ [14]	$C_{P,d} = 0.94C_P = 2124$ [14]
Charred (above 300 °C)	$k_c = 0.35k = 0.09$ [14]	$\rho_c = 0.19\rho = 128$ [14]	$C_{P,c} = 0.69C_P = 1559$ [14]

Initially, a Neumann boundary condition was applied on the exposed surface as shown in Equation 1. The rear surface was assumed to be adiabatic since the measured temperature rise at the back of each sample was minimal, so the assumption of semi-infinite heating is valid.

$$x = 0: \alpha\dot{q}''_e - \dot{q}''_{l,c} - \dot{q}''_{l,r} - k\frac{\partial T}{\partial x} = \rho C_P\, dx\frac{\partial T}{\partial t}$$

$$x = 0: \alpha\dot{q}''_e - h_c(T_s - T_\infty) - \varepsilon\sigma\left(T_s{}^4 - T_\infty{}^4\right) - k\frac{\partial T}{\partial x} = \rho C_P\, dx\frac{\partial T}{\partial t} \quad (1)$$

For the two lowest heat fluxes of 5 and 10 kW/m^2, the inert solution with ambient properties provides quite a close approximation to the experimental values. There are some minor divergences due to the effects of moisture, which are still present for the perpendicular heating case (though much less significant than in parallel heating) and are not accounted for in the model. This can be seen in Figure 6 in the evolution of temperatures at various depths under 5 and 10 kW/m^2, as the experimental temperatures initially rise faster, before the model begins to over-predict temperatures in the deeper thermocouples around 100 °C. Nevertheless, Figure 7 shows that the inert solution provides a good prediction of temperature profiles for both of these heat fluxes at all time-intervals between 5 and 60 minutes of exposure. From these profiles, the maximum error after 60 minutes at 10 kW/m^2 is about 18 °C, or 16 % of the temperature rise above ambient, occurring at a depth of 25 mm from the heated surface. The corresponding values for 5 kW/m^2, occurring at a depth of 15 mm, are 11 °C or 10 % of temperature rise.

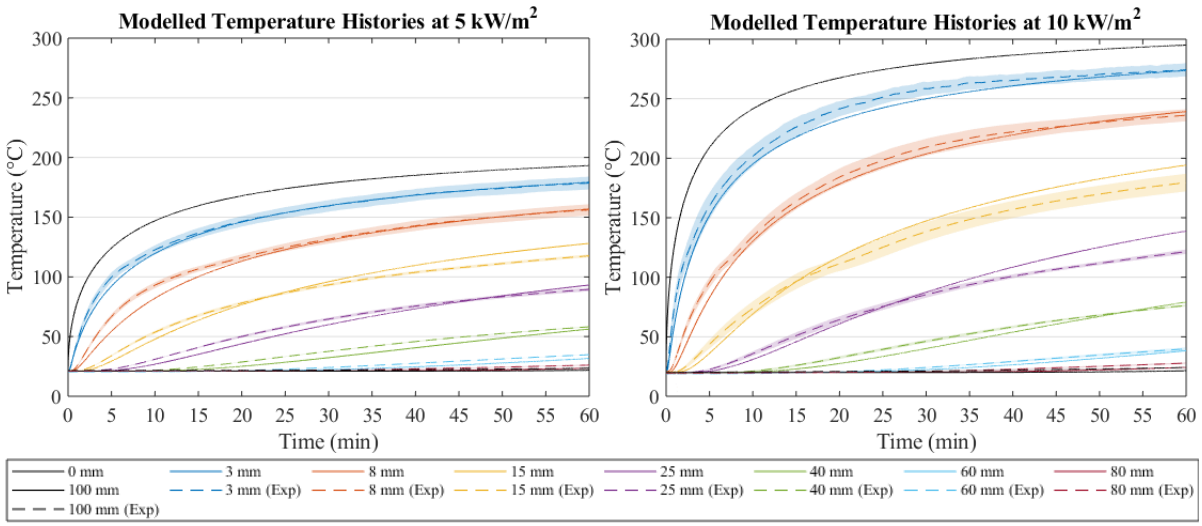

Figure 6. Temperatures at various depths under 5 and 10 kW/m^2 irradiation, by inert heat-transfer modelling (solid) and experimental results (dashed) with standard deviation intervals shaded.

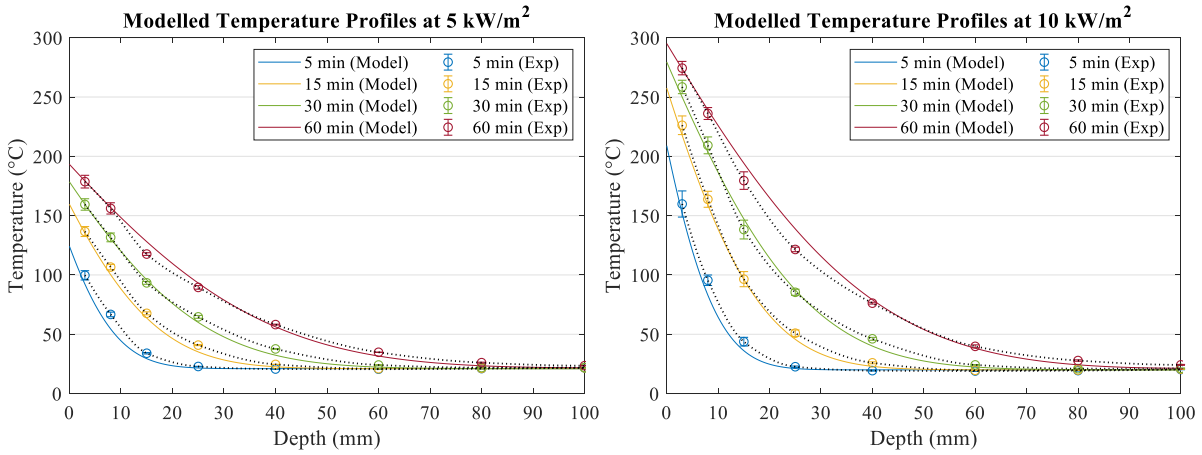

Figure 7. In-depth temperature profiles under 5 and 10 kW/m^2 irradiation, by inert heat-transfer modelling (solid) and experimental results (circles) with standard deviation intervals indicated.

The inert heating regime diverges greatly from reality for the higher radiant heat fluxes of 30 and 60 kW/m^2, with temperatures under-predicted by the model at all depths, particularly for the shallower locations where the difference could be hundreds of degrees. While expected, these results suggest that the exothermic effects of char oxidation, increased thermal diffusivity of the char layer, and increased thermal exposure (due to surface flaming, cracking, and regression) appear to dominate over the endothermic effects of moisture evaporation and anaerobic pyrolysis. Surface flaming, which was present in the 60 kW/m^2 heating regime, can provide a significant additional heat flux at the surface of the sample, and has previously been characterised to be within the range of 20-40 kW/m^2.[22]

While the magnitude of this heat flux has not been determined for the present case, its effect may be accounted for indirectly by adjusting the model to utilise the experimentally measured temperatures at the shallowest depth (3 mm from the heated surface) as a Dirichlet boundary condition for heat diffusion through the rest of the material. This allows minimising the uncertainty caused by the near-surface phenomena of flaming, cracking and regression, so

that the contributions of the condensed phase reactions and changing material properties may be observed separately. This approach is limited by the fact that the shallowest thermocouples eventually become exposed and fall out, meaning that they can no longer be relied upon as a boundary condition. For both 30 and 60 kW/m^2 heating, this occurs after approximately 20 minutes, so this experimental data has only been used as a model input up to this time. Additionally, the model may utilise only constant thermal properties, or it may account for different properties corresponding to physical and chemical changes in the material. The first case, called model "M1", assumes that the ambient material properties apply throughout heating. The second model, "M2", allocates different thermal properties to the "wet zone" (below 100 °C), the "dry zone" (between 100 and 300 °C) and the "char layer" (above 300 °C) as shown in Table 2. These changing properties are not yet well established for bamboo, however the chemical composition of bamboo is similar to that of timber,[7] so the "dry" and "char" layer properties have been estimated as fractions of the ambient material properties, based on the equivalent fractions used for timber.[14]

When these models are compared with the experimental results, as shown in Figure 8, it can be seen that there is still significant divergence. This is seen initially around 100 °C as the model fails to account for endothermic moisture evaporation, which delays the initial temperature rise in the experimental results. However, this effect is reversed as temperatures rise further, with the rate of temperature rise in the models reducing significantly compared to the experimental case above 300 °C. Eventually, the modelled temperatueres fall back below the experimental values, and remain significantly lower as a quasi-steady state is approached. Model M2, which accounts for changing material properties, predicts higher temperatures than M1, particularly due to the higher thermal diffusivity of the char layer, however this does not account for the eventual difference between the modelled and experimental values. This is likely due to exothermic char oxidation reactions occurring above 400 °C,[20] which have not been accounted for in the models.

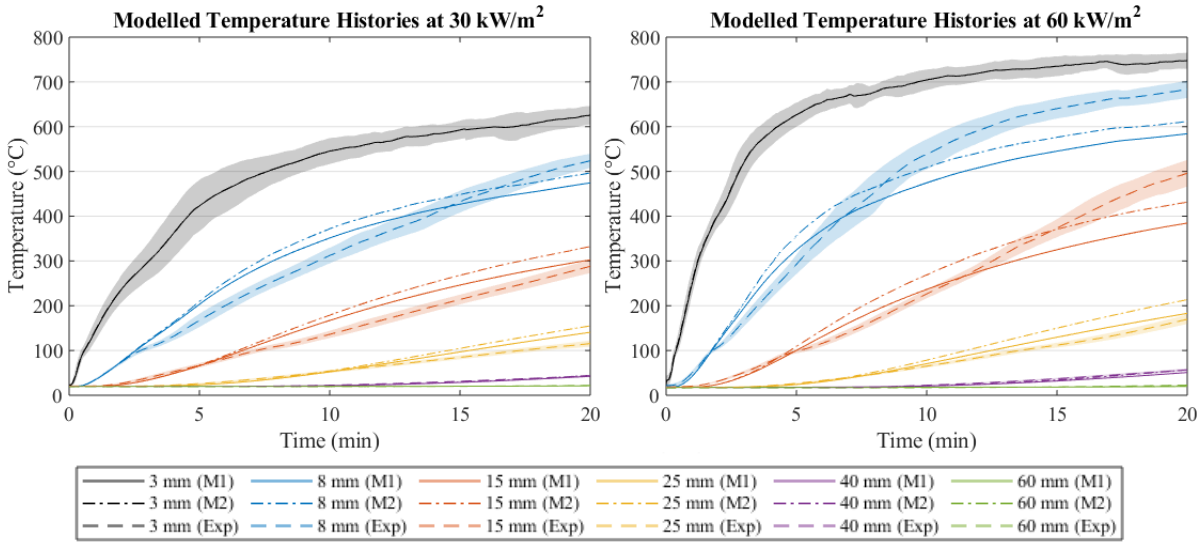

Figure 8. Temperatures at various depths under 30 and 60 kW/m^2 irradiation, by models with measured temperature boundary conditions and constant material properties (M1, solid) or properties varying across moving boundaries (M2, dash-dot), compared with experimental results (dashed).

This exothermic oxidation effect has previously been found to have a significant influence on

temperatures in timber,[12,14,23] and may explain why heat diffusion alone is underpredicting the temperatures at 30 and 60 kW/m^2. A simplified method has been used to evaluate the relative contributions of different reactions occurring within the material, by assuming that they occur at an infinite rate at discrete moving temperature boundaries. This is based on the moving boundary model used by Reszka,[12] and it allows the different source terms in the heat transfer model to be estimated and benchmarked against the amount of energy being conducted through the material at these boundaries. The intent of this analysis is to determine which (if any) source terms may be ignored, and which terms will need to be investigated further and accounted for in a future model. Following this method, the speed at which each boundary isotherm (B_j) moves is multiplied by the fractional density (ρ_i) of the species (i) that is reacting, and by the heat of the reaction (ΔH_j), to calculate a 'reaction heat flux' ($\dot{q}''_j$) that is applied at each boundary, as per Equation 2.

$$\dot{q}''_j = \rho_i \, \Delta H_j \, \frac{dB_j(t)}{dt} \tag{2}$$

The fractional densities are based on the proportions of water, dry bamboo and char presented in Table 2, while the heats of reaction have been taken as values found for wood.[12,14] The evaporation and pyrolysis boundaries have been taken as the 100 °C and 300 °C isotherms, respectively. Char oxidation occurs at a varying rate over a wide range of temperatures, depending on the heating rate and availability of oxygen.[20] At lower heating rates, char oxidises between 400 to 500 °C, but may oxidise at temperatures over 600 °C under higher heating rates.[6] For the purpose of estimating the overall contribution of this source term, the oxidation boundary was assumed to be at 600 °C – towards the upper end of this range – since the source terms will be analysed for the relatively high heat flux of 60 kW/m^2. The movement of these boundaries has been estimated from the experimental results for 5, 30 and 60 minutes after exposure, to evaluate how the size of the source term changes over time. However, instantaneous boundary movement speeds may be unreliable since they must be calculated from interpolation between measurement points. To account for this uncertainty, ranges of periodic movement speeds were calculated based on the movement of the isotherms over the five-minute intervals immediately before and after the specified times (up to 60 minutes). The temperature gradient at each boundary has also been used to estimate the heat being conducted through the boundary, according to Equation 3, for comparison with the reaction fluxes. These gradients are similarly based on the interpolated temperature profiles, with finite temperature differences estimated over one millimetre either side of the isotherm, so there is a degree of error associated with these approximations as well.

$$\dot{q}''_{cond} = - k_i \frac{\Delta T}{\Delta x} \tag{3}$$

The results of this analysis, which are summarised in Table 3, suggest that the exothermic char oxidation reaction is far more significant than the endothermic effects of evaporation and pyrolysis. In each case, the maximum reaction and conduction heat fluxes are achieved for the earlier times, before reducing as a quasi-steady state is approached.

Table 3. 60 kW/m^2 – Endothermic (Negative) and Exothermic (Positive) Boundary Source Terms and Heat Conduction under a Moving Boundary Layer Assumption

Time (min)	**Boundary movement** (mm/min)	**Fractional density** (kg/m^3)	**Heat of reaction** (kJ/kg)	**Reaction heat flux** (kW/m^2)	**Temperature gradient** (K/mm)	**Thermal conductivity** (W/mK)	**Conduction heat flux** (kW/m^2)
100 °C isotherm – Evaporation							
5	1.30 – 3.00	47 (water)	-2410 [14]	(-) 2.5 – 5.7	13	0.25	3.3
30	0.80 – 0.85			(-) 1.5 – 1.6	6		1.5
60	0.45			(-) 0.8	5		1.3
300 °C isotherm – Pyrolysis							
5	1.05 – 1.55	628 (dry bamboo)	-418 [12]	(-) 4.6 – 6.8	45	0.24	10.8
30	0.75 – 0.80			(-) 3.3 – 3.5	20		4.8
60	0.70			(-) 3.1	17		4.1
600 °C isotherm – Char oxidation							
5	0.60 – 0.65	128 (char)	37700 [14]	48.3 – 52.3	82	0.09	7.4
30	0.30 – 0.40			24.1 – 32.2	26		2.3
60	0.25			20.1	15		1.4

The endothermic evaporation and pyrolysis terms are of a similar magnitude to the amount of energy being conducted through the material at these locations, with conduction being slightly larger than the pyrolysis term. However, the amount of energy generated by exothermic oxidation ranges from 7 to 14 times greater than the heat being conducted through this point in the char layer, and the relative difference between these terms increases over time. This would explain why there is such a significant divergence between the models and the experimental results for high temperatures. Accounting for the endothermic phenomena should reduce the overprediction of temperatures in the model before oxidation begins to occur, but it would appear that these effects are secondary in comparison to the influence of the exothermic reaction at higher heat fluxes. The reduction over time of the ratio between the evaporative term and the conducted energy also agrees well with the experimental observations, as the inflexion in the temperature curves near 100 °C appears to decrease in significance at greater depths.

5. CONCLUSIONS

A series of experiments have been conducted to measure the in-depth heating of laminated bamboo samples subjected to different radiant heat fluxes. These heat fluxes, at 5, 10, 30 and 60 kW/m^2 were chosen to induce different phenomena within the material, so that the effects of these can be isolated and evaluated separately. Heat transfer models of different levels of complexity have been used to assess the significance of the different energy source terms that arise under different heating conditions, and these models have been compared with the experimental results. Analysis of the experimental and modelling results has identified several distinct phenomena that occur under different conditions. It was found that there is a clear distinction between the behaviour of laminated bamboo when heated perpendicular or parallel to the grain, beyond that which can be explained by the different thermal conductivities in each direction. Moisture migration along the grain becomes a critical factor when bamboo is heated in this direction, resulting in increased convective heat transfer to deeper parts of the material, and an accumulation of moisture in depth that

accentuates the endothermic plateau in the temperature profiles around 100 °C. This migration of moisture is not observed when the heat is applied perpendicular to the grain, because the orientation of the fibres and glue layers inhibit this. Any heat transfer model of parallel heating would need to account for this mass transfer effect, but this may not be necessary for heating perpendicular to the grain, which is the most common scenario for bamboo structures.

Charring rates at 60 kW/m^2 were similar for both the perpendicular and parallel heating orientations, with average rates after 60 minutes of 0.74 and 0.70 mm/min, respectively. The heated depth was significant in either case, but became much larger for parallel heating due to the additional convective heating effect of moisture migration along the fibres, as well as the higher thermal diffusivity in this direction. Even for the perpendicular heating case, the thickness of the heated layer continued to grow throughout the full 60 minutes of exposure, at which time the 60 °C isotherm was 29 mm ahead of the charring front. This indicates that the deterioration of mechanical properties in the material may not be accurately predicted by a standard reduced cross-section method with an assumed constant zero-strength layer.

The experimental results for perpendicular heating showed a good agreement with purely inert diffusive heating models for 5 and 10 kW/m^2 irradiation, where no significant pyrolysis was observed beyond the surface of the material. This validates the use of a simple heat diffusion equation for modelling regions of the material below around 300 °C, however there was a divergence between this model and experimental results for higher temperatures. At 30 and 60 kW/m^2, the experimental results rose significantly higher than the predicted temperatures above 400 °C, even when boundary effects such as flaming, cracking and surface regression were isolated. This disparity is likely due to the dominance of exothermic char oxidation reactions at temperatures above 400 °C, which was also highlighted in a simple comparative analysis of different energy source terms and conductive heat fluxes at different temperatures. Therefore, any model of in-depth temperatures in laminated bamboo under fire conditions must account for the additional thermal loads from oxidation and surface flaming to provide accurate and conservative predictions for thermo-mechanical structural analysis. This in turn requires understanding the ventilation conditions of the fire, since this will determine the available oxygen and potential for direct flame impingement. Including the endothermic source terms should further improve the accuracy of a future model, but since their magnitude is much smaller and comparable to conductive heat fluxes, it may be more efficient to account for these terms through ‘effective’ thermal properties near the boundary layers. Future work should include specific quantification of the changing material properties and source terms that are characteristic of laminated bamboo, so that these may be included in a simple moving boundary model.

ACKNOWLEDGEMENTS

The authors would like to thank Moso International BV for providing the laminated bamboo for this project, as well as the financial support provided by the Worshipful Company of Engineers through the Sir Peter Gadsden Britain Australia Travel Award 2018. The authors are also grateful for the assistance of Jeronimo Carrascal, Mateo Gutierrez, Angela Solarte and the rest of the UQ Fire team.

REFERENCES

1. Sharma B, Gatoo A, Bock M, Ramage M. Engineered bamboo for structural applications. *Construction and Building Materials* 2015;81:66-73.
2. Sharma B, Gatoo A, Bock M, Mulligan H, Ramage M. Engineered bamboo: state of the art. *Construction Materials* 2015;168(CM2):57-67.
3. Reszka P, Torero JL. Fire behaviour of timber and lignocellulose. In Belgacem N & Pizzi A, eds. *Lignocellulosic Fibers and Wood Handbook*, Scrivener Publishing LLC; 2016:555-581.
4. EN 1995-1-2. Eurocode 5. Design of timber structures – Part 1-2: General – Structural fire design. Brussels: European Committee for Standardization; 2004.
5. White RH. Analytical Methods for Determining Fire Resistance of Timber Members. In Hurley MJ et al. eds. *SFPE Handbook of Fire Protection Engineering*. 5th ed. Springer, New York; 2016:1979-2011.
6. Bartlett AI, Hadden RM, Bisby LA. A review of factors affecting the burning behaviour of wood for application to tall timber construction. *Fire Technology* 2019;55(1):1-49.
7. Scurlock JMO, Dayton DC, Hames B. Bamboo: an overlooked biomass resource?. *Biomass and Bioenergy* 2000;19(4):229-244.
8. Gutierrez Gonzalez M, Madden J, Maluk C. Experimental study on compressive and tensile strength of bamboo at elevated temperatures, *2018 World Conference on Timber Engineering*. WCTE 2018 Committee, Seoul, Republic of Korea, 20-23 August 2018.
9. Bartlett AI, Chapman A, Roberts C, Wiesner F, Hadden RM, Bisby LA. Thermal and flexural behaviour of laminated bamboo exposed to severe radiant heating, *2018 World Conference on Timber Engineering*, WCTE 2018 Committee, Seoul, Republic of Korea, 20-23 August 2018.
10. Solarte A, Numapo J, Hidalgo JP, Torero JL. Flame spread in laminated bamboo structures, *Proceedings of the Ninth International Seminar on Fire and Explosion Hazards (ISFEH9)*. Saint-Petersburg Polytechnic University Press, Saint Petersburg, Russia, 2019;755-766.
11. Shah DU, Bock MCD, Mulligan H, Ramage MH. Thermal conductivity of engineered bamboo composites. *Journal of Materials Science* 2016;51(6):2991-3002.
12. Reszka P. In-depth temperature profiles in pyrolysing wood. PhD thesis, The University of Edinburgh, Edinburgh, 2008.
13. Richter F, Atreya A, Kotsovinos P, Rein G. The effect of chemical composition on the charring of wood across scales. *Proceedings of the Combustion Institute* 2019;37(3):4053-4061.
14. Lautenberger C, Fernandez-Pello C. A model for the oxidative pyrolysis of wood. *Combustion and Flame* 2009;156:1503-1513.
15. Lautenberger C. A generalized pyrolysis model for combustible solids. PhD thesis, The University of California Berkeley, Berkeley, 2007.
16. Bal N. Uncertainty and complexity in pyrolysis modelling. PhD thesis, The University of Edinburgh, Edinburgh, 2012.
17. Friquin KL. Material properties and external factors influencing the charring rate of solid wood and glue-laminated timber. *Fire and Materials* 2011;35:303-327.
18. Solarte A, Hidalgo JP, Torero JL. Flammability studies for the design of fire-safe bamboo structures, *2018 World Conference on Timber Engineering*, WCTE 2018 Committee, Seoul, Republic of Korea, 20-23 August 2018.
19. ISO 5660-1:1993. Fire Tests Reaction to Fire Part 1: Rate of Heat Release from Building Products (Cone Calorimeter Method). International Organization for Standardization, Geneva; 1993.

20. Ohlemiller TJ, Kashigawi T, Werner K. Wood gasification at fire level heat fluxes. *Combustion and Flame* 1987;69(2):155-170.
21. Incropera FP, DeWitt DP, Bergman TL, Lavine AS. *Fundamentals of heat and mass transfer*. 6th ed. Hoboken, NJ: John Wiley & Sons; 2007.
22. McCoy CG, Tilles JL, Stoliarov SI. Empirical model of flame heat feedback for simulation of cone calorimetry. *Fire Safety Journal* 2019;103:38-48.
23. Boonmee N, Quintiere JG. Glowing ignition of wood: the onset of surface combustion. *Proceedings of the Combustion Institute* 2005;30:2303-2310.